


Unexpected behavior of the crystal growth velocity at the hypercooling limit

P. Fopp¹,* M. Kolbe, F. Kargl,[†] and R. Kobold[‡]

Institut für Materialphysik im Weltraum, Deutsches Zentrum für Luft- und Raumfahrt (DLR), 51170 Köln, Germany

W. Hornfeck

Institute of Physics of the Academy of Sciences of the Czech Republic, Na Slovance 2, 18221 Prague, Czech Republic

 (Received 19 November 2018; revised 14 November 2019; accepted 23 December 2019; published 27 July 2020)

The crystal growth velocity is one thermodynamic parameter of solidification experiments of undercooled melts under nonequilibrium conditions, which is directly accessible to observation. We applied the electrostatic levitation technique in order to study the crystal growth velocity v as a function of the undercooling ΔT for the intermetallic, congruently melting binary alloy NiTi and the glass-forming alloy Cu–Zr, as well as for the Zr-based ternary alloys $(\text{Ni}_x\text{Cu}_{1-x})\text{Zr}$ ($x = 0.3, 0.4$) and the Ni-based ternary alloy $\text{Ni}(\text{Zr}_{0.5}\text{Ti}_{0.5})$. All investigated systems within this work, except the eutectics $\text{Cu}_{0.56}\text{Zr}_{0.44}$ and $\text{Cu}_{0.46}\text{Zr}_{0.54}$, exceeded the hypercooling limit ΔT_{hyp} and, remarkably, every $v(\Delta T)$ relation changed significantly at ΔT_{hyp} . Our results for glass-forming CuZr indicate that the influence of the diffusion coefficient $D(T)$ on $v(\Delta T)$ at high undercoolings, as claimed in literature, cannot be the sole reason for the existence of a maximum in the $v(\Delta T)$ behavior. These observations could make a valuable contribution concerning an extension of growth theories to undercooling temperatures $\Delta T > \Delta T_{\text{hyp}}$. Nevertheless, our finding has direct consequences to various disciplines, as our earth and all living beings are examples for nonequilibrium systems. The scatter of our velocity data is at least two orders of magnitude smaller than measurements performed by former works due to our experimental setup, which allowed precise contactless triggering at a specific undercooling, and our analysis method, which considered the respective solidification morphologies.

DOI: [10.1103/PhysRevMaterials.4.073405](https://doi.org/10.1103/PhysRevMaterials.4.073405)

I. INTRODUCTION

Levitation techniques offer the opportunity to investigate the solidification behavior of metallic melts within a broad undercooling regime [1–4]. In general, the higher the cooling rate, the higher undercoolings can be achieved. However, to extend the undercooling range significantly, the cooling rates have to be increased by orders of magnitude. Electrostatically levitated freely suspended single-component metallic melts usually exhibit cooling rates of about 200–400 Ks^{-1} , whereas even at the same temperature binary and multicomponent systems exhibit cooling rates which are $< 200 \text{Ks}^{-1}$. Their different cooling rates originate from the properties of the systems, e.g., their different specific-heat capacities c_p . Despite of their small cooling rates in the electrostatic levitator (ESL), some metallic melts, especially multicomponent systems, can reach such high undercoolings that the temperature of the melt passes the glass transition temperature T_g . At T_g the structure of the melt is preserved and no change in the enthalpy H_f can be observed. In this case, the as-solidified sample exhibits an amorphous structure. For the alloys investigated,

the solidification is accompanied by a sufficient change in the enthalpy to be observed by the unaided eye as sudden change in brightness of the levitating sample. With a high-speed camera, the onset and end of solidification can be clearly pinpointed on the sample surface (Fig. 1), which makes it possible to determine the (surface) solidification velocity as a function of the undercooling $v(\Delta T)$. If a broad undercooling regime is accessible, one can investigate, e.g., the influence of temperature-dependent thermodynamic parameters on the $v(\Delta T)$ curve [5,6].

CuZr is an alloy which can form a metallic glass and has recently been investigated with respect to its dendrite growth dynamics [6,7]. Most notably, Tang and Harrowell reported an anomalously slow crystal growth of CuZr at high undercooling temperatures [8]. In [6] it is claimed that at high undercooling temperatures the diffusion coefficient $D(T)$ becomes dominant in comparison to the driving force for solidification, leading to a decrease in the slope, which ultimately becomes negative at even higher undercoolings, of the $v(\Delta T)$ curve. This leads to a maximum in $v(\Delta T)$. If the temperature of the undercooled melt is approaching T_g , the characteristics of the dendrite growth kinetics changes. Similar results have already been presented for nonmetallic glass formers, e.g., the organic tris-(naphthylbenzene) [9].

For most systems the glass transition temperature is far away from the undercoolings which can be achieved. For binary systems it is possible to reach T_g , although still very difficult, especially with levitation techniques due to the limited cooling rate. The alloys investigated within this work tend

*patrick.fopp@dlr.de

[†]Also at Foundry Institute, Faculty of Georesources and Materials Engineering, RWTH Aachen University, 52062 Aachen, Germany.

[‡]Also at Programmatik Raumfahrtforschung und -technologie, Deutsches Zentrum für Luft- und Raumfahrt (DLR), 51170 Köln, Germany; raphael.kobold@dlr.de

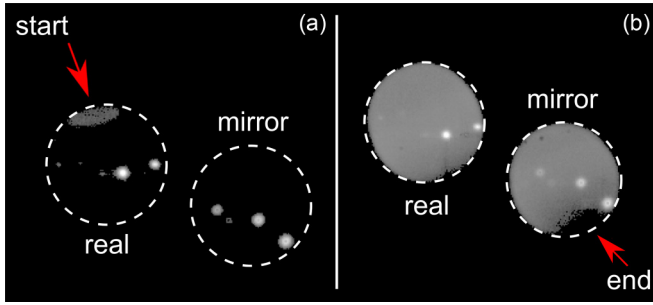


FIG. 1. Illustration of two HSC frames, which show (a) the starting point of the solidification on the front side of the sample and (b) the moment shortly before the end of solidification on the back side. A mirror installed in the levitation furnace allows to observe $\approx 98\%$ of the sample surface, which makes it possible to accurately determine the time frame between start and end of the solidification, even for rotating samples.

to undercool up to 300–400 K below their equilibrium melting temperature T_m . This temperature range is still far away from T_g , but is sufficient for the melt to pass through the so-called *hypercooling limit*, which is thermodynamically defined as

$$\Delta T_{\text{hyp}} = \frac{\Delta H_f}{c_p}, \quad (1)$$

where complete isenthalpic solidification is achieved. For $\Delta T < \Delta T_{\text{hyp}}$ the heat of fusion ΔH_f , which is released during the solidification process, is sufficient to raise the temperature of the sample to T_m . In this case, a certain amount (depending on the undercooling) of the material crystallizes in the time frame of the recalcence, whereas the residual melt solidifies under equilibrium conditions. In the case of $\Delta T > \Delta T_{\text{hyp}}$, ΔH_f is not sufficient to raise the temperature of the sample to T_m and the melt crystallizes completely in the process of recalcence.

In 1900, Wilson already expressed his thoughts about the existence of a hypercooling limit [10]. In the 1960s Glicksman *et al.* described the hypercooled region [11] and mentioned the idea of a supercooled solid-liquid interface if ΔT_{hyp} is exceeded [12]. Schillings investigated solidification processes of pure and binary organic model substances, e.g., succinonitrile and succinonitrile-acetone [13]. Solidification from deep undercoolings is an up-to-date topic also in water research [14–16]. Only recently, Buttersack *et al.* reported about a new value for the hypercooling temperature of water [17]. In the late 1990s Wilde *et al.* and Volkman *et al.* mentioned ΔT_{hyp} for completely miscible Pd-based alloys [18,19]. The solidification velocity as a function of the undercooling was measured by Volkman *et al.* with a short remark that passing the hypercooling limit has *no influence* on $v(\Delta T)$ [19]. However, our findings raise doubts about this point. Notably, Wilde was the first to recognize a flattening of the $v(\Delta T)$ curves of $\text{Co}_{80}\text{Pd}_{20}$ and $\text{Co}_{50}\text{Pd}_{50}$ for undercoolings above ΔT_{hyp} measured in the EML by Volkman *et al.* [20]. He interpreted that the temperature independence of the growth velocity in the hypercooling regime originates from the growth mechanism for undercoolings above the hypercooling limit and remarked that a theoretical discussion was lacking at the time of his

work. The scatter of our velocity data (y axes of Figs. 3–5) is at least two orders of magnitude smaller than the velocity measurements performed by Volkman *et al.*, which used photodiodes with electronic amplification.

In this work, we present experimental evidence for the influence of the hypercooling limit ΔT_{hyp} on $v(\Delta T)$ for the binary intermetallic alloys NiTi and CuZr, as well as for the ternary compositions $(\text{Ni}_{0.3}\text{Cu}_{0.7})\text{Zr}$, $(\text{Ni}_{0.4}\text{Cu}_{0.6})\text{Zr}$, and $\text{Ni}(\text{Zr}_{0.5}\text{Ti}_{0.5})$.

II. EXPERIMENT

High-purity elements (Zr: 99.97 %, Smart Elements; Ni: 99.995 %, Alfa Aesar; Ti: 99.995 %, Smart Elements; Cu: 99,999 %, Smart Elements) are prepared and alloyed by arc melting in a protective argon (6N) atmosphere yielding spherical samples with a diameter of 3–4.5 mm. The mass loss during arc melting is found to be less than 0.2 mg. During the levitation experiment, the mass loss is monitored by a vacuum meter and is expected after the experiment to less than 0.4 mg for all alloys. Thus, the initial compositions are not changed significantly.

A spherical sample is placed in an electrode system of an electrostatic levitator and is levitated and subsequently heated with a Mergenthaler ML75 infrared heating laser ($P = 75 \text{ W}$, $\lambda = 808 \text{ nm}$) under ultra-high-vacuum conditions (10^{-8} mbar). For a detailed description of the functionality of the ESL, the reader is referred to Refs. [1,21,22]. The temperature is measured contactlessly with a two-color pyrometer integrated into a Mergenthaler LH500-M laser head (10 kHz, wavelength range 1600–1950 nm, temperature range 410°C – 1410°C , accuracy 0.3 % of measured value or $\pm 2^\circ\text{C}$).

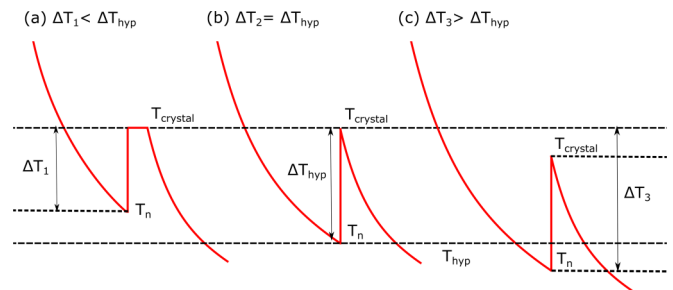


FIG. 2. TTPs for three different undercoolings T_n illustrating the transition between $\Delta T_1 < \Delta T_{\text{hyp}}$ and $\Delta T_3 > \Delta T_{\text{hyp}}$ as it is observed for all systems investigated in this work. The time frame of the recalcence varies between 2 ms (NiTi) and 40 ms (Cu–Zr). (a) At low and medium undercoolings $\Delta T_1 < \Delta T_{\text{hyp}}$ the latent heat that is released during solidification raises the sample temperature T_{crystal} up to the melting temperature T_m . A part of the sample solidifies during the recalcence under nonequilibrium conditions. The rest solidifies in equilibrium in the melting plateau. (b) If the released latent heat is just sufficient to raise T_{crystal} up to T_m , the melting plateau vanishes. The specific undercooling temperature for this scenario corresponds to the hypercooling limit $\Delta T_2 = \Delta T_{\text{hyp}}$. (c) For high undercoolings $\Delta T_3 > \Delta T_{\text{hyp}}$ the latent heat is not sufficient anymore to raise T_{crystal} up to T_m and 100 % of the sample solidifies under nonequilibrium conditions.

TABLE I. Enthalpies of fusion ΔH_m , specific-heat capacities of the liquid at T_m at constant pressure $c_{p,1}$, calculated hypercooling limits $\Delta T_{\text{hyp,calc}} = \Delta H_m/c_{p,1}$, experimentally found hypercooling limits $\Delta T_{\text{hyp,expt}}$ (extracted from the TTPs), maximum achieved undercooling temperatures ΔT_{max} , the errors for the highest measured velocities Δv , and the used frame rates for the HSC in fps. The asterisk denotes that our own values were taken instead of literature values from [31] [$\text{Cu}_{0.46}\text{Zr}_{0.54}$: (40.3 ± 0.7) J/mol K; CuZr : (32.6 ± 2.3) J/mol K; $\text{Cu}_{0.46}\text{Zr}_{0.54}$: (38.4 ± 0.7) J/mol K] for the calculation of $\Delta T_{\text{hyp,calc}}$. The double asterisk denotes the error of ΔH_m was estimated by interpolation of the errors for ΔH_m of $\text{Cu}_{0.56}\text{Zr}_{0.44}$ and $\text{Cu}_{0.46}\text{Zr}_{0.54}$.

System	T_L (K)	ΔH_m (kJ/mol)	$c_{p,1}$ (J/mol K)	$\Delta T_{\text{hyp,calc}}$ (K)	$\Delta T_{\text{hyp,expt}}$ (K \pm 10 K)	ΔT_{max} (K \pm 10 K)	Δv (cm/s)	fps (1/s)
$\text{Cu}_{0.56}\text{Zr}_{0.44}$	1163	$13.7^a \pm 0.3^a$	$40.4^{**} \pm 0.7^{**}$	339 ± 1.6		230	± 0.2	500
CuZr	1208	$9.2^b \pm 0.35^{**}$	$39.7^d \pm 0.6^d$	232 ± 5.5	230	280	± 0.2	500
$\text{Cu}_{0.46}\text{Zr}_{0.54}$	1201	$12.5^a \pm 0.4^a$	$39.3^{**} \pm 0.5^{**}$	318 ± 6.3		270	± 0.2	500
$(\text{Ni}_{0.3}\text{Cu}_{0.7})\text{Zr}$	1039	11.1 ± 0.5	$41.2^d \pm 0.3^d$		270	320	± 0.5	500
$(\text{Ni}_{0.4}\text{Cu}_{0.6})\text{Zr}$	1072	10.6 ± 1.1	$37.8^d \pm 2.4^d$		280	350	± 0.1	2000
NiZr	1533 ^c	14.7 ± 0.2	$42.6^c \pm 0.3^c$	$346^c \pm 2.3^c$		300	± 0.5	10000
$\text{Ni}(\text{Zr}_{0.5}\text{Ti}_{0.5})$	1260	15.6 ± 0.6	$46.3^d \pm 0.3^d$		337	360	± 0.5	6000
NiTi	1310	12.5 ± 0.5	$35.7^d \pm 0.3^d$		350	390	± 0.8	20000

^aReference [31].

^bReference [5].

^cReference [24].

^dThe $c_{p,1}$ values were calculated from the cooling curves of the experiment and averaged. The ΔH_m values were then determined via $\Delta H_m = \Delta T_{\text{hyp,expt}} \times c_{p,1}$. The errors for ΔH_m are within ± 0.2 kJ/mol and for $c_{p,1}$ within ± 0.3 J/mol K [for $(\text{Ni}_{0.4}\text{Cu}_{0.6})\text{Zr}$: ± 1 kJ/mol and ± 2.4 J/mol K].

A typical ESL cycle consists of the following temperature steps: the solid sample is heated up to T_m . For congruently melting systems, the temperature remains constant during the melting process, yielding a plateau in the temperature-time profile (TTP). If the sample is completely liquid, the temperature of the melt is further increased in order to evaporate possible contaminants. Subsequently, the infrared laser is switched off and the sample cools down only through radiation of heat. Due to the absence of crucible walls, heterogeneous nucleation is being suppressed and the sample undercools well below T_m with a mean material-specific cooling rate $\Delta T/\Delta t$. At some point, i.e., at the nucleation temperature T_n , the solidification sets in along with the release of latent heat, which increases the sample temperature. Due to the steep recalescence in the TTP, T_n can be pinpointed with high accuracy (see Fig. 2).

With a high-speed camera (HSC) Photron Ultima APX 775k the crystallization of the liquid sample is recorded in order to ensure that only a single crystallization event occurs in every ESL cycle. Table I shows the frame rates that were used for the different alloy systems due to their differing growth velocities. For all cases, a field of view of 512×320 pixel is chosen with a resolution of ≈ 30 $\mu\text{m}/\text{pixel}$.

III. RESULTS AND DISCUSSION

It was found that the solidification fronts are spherical for undercoolings $\Delta T > \Delta T_{\text{hyp}}$ and can be approximated by a spherical shape for $\Delta T < \Delta T_{\text{hyp}}$, respectively. Therefore, the time between the first and last frame (FL method) was used to determine the velocities. A spherical front is assumed to be formed by numerous dendrites growing in all directions, i.e., it is most likely that a dendrite grows between the onset and end of solidification, which justifies using the FL method to determine the dendrite growth velocity as a function of the

undercooling. Accordingly, the $v(\Delta T)$ data were calculated with the ratio of the sample diameter d_s and the time Δt between the first and last frame of the HSC recording, i.e., $v(\Delta T) = d_s/\Delta t$.

Our $v(\Delta T)$ results for CuZr in Fig. 3 indicate that there is no continuous decrease in slope of the $v(\Delta T)$ curve at higher undercoolings as proposed in [5,6]. Wang *et al.* state that in glass-forming systems the mobility of the atomic movement rapidly decreases if the undercooling approaches the glass temperature. The steep rapid decrease of the diffusion coefficient $D(T)$ should overcome the acceleration of the

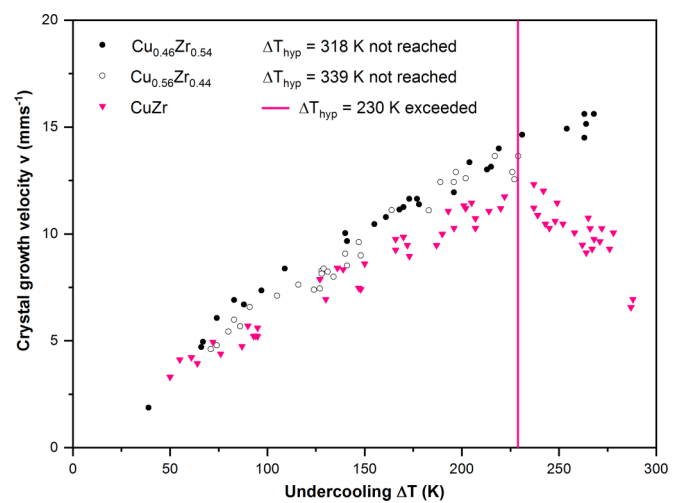


FIG. 3. Crystal growth velocity v as a function of the undercooling ΔT measured for intermetallic CuZr and the two adjacent eutectics $\text{Cu}_{0.56}\text{Zr}_{0.44}$ and $\text{Cu}_{0.46}\text{Zr}_{0.54}$. While the $v(\Delta T)$ curve increases for both eutectics within the whole obtained undercooling regime, the curve for intermetallic CuZr increases until $\Delta T_{\text{hyp}} = 230$ K (vertical pink line) and then decreases with increasing undercooling.

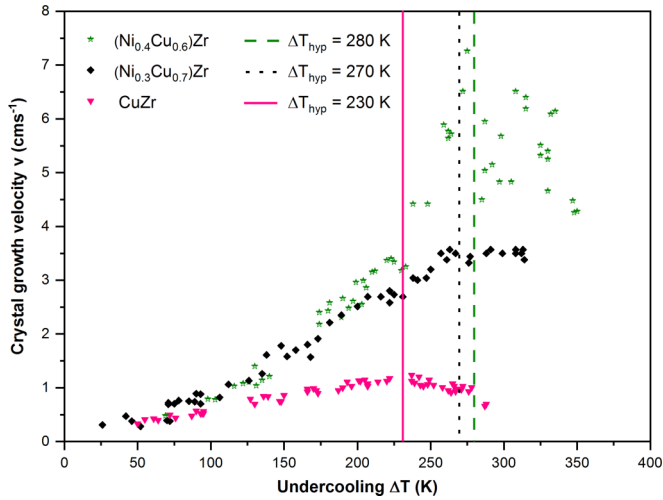


FIG. 4. Crystal growth velocity v as a function of the undercooling ΔT measured for the Zr-based ternary alloys $(\text{Ni}_{0.3}\text{Cu}_{0.7})\text{Zr}$ and $(\text{Ni}_{0.4}\text{Cu}_{0.6})\text{Zr}$. One can see that, with increasing Ni at. %, the velocity increases faster for $\Delta T < \Delta T_{\text{hyp}}$ and ΔT_{hyp} shifts to higher undercooling temperatures. As observed for CuZr, the $v(\Delta T)$ relations for the ternary alloys exhibit a sudden change at ΔT_{hyp} .

interface [caused by the increasing driving force $\Delta G(T)$] at a specific undercooling $\Delta T = 140$ K, resulting into a maximum of the $v(\Delta T)$ curve at $\Delta T \approx 225$ K [6]. In fact, we observe a kink in the curve of the solidification velocity at a specific undercooling temperature. No discrete change of the solidification front geometry is observed in the HSC recordings and hence this can be ruled out as being the cause of the observed deceleration. Remarkably, experiments we have carried out on a number of other systems corroborate our finding that the changes in the $v(\Delta T)$ relations can unambiguously be correlated with reaching the hypercooling limit (Figs. 3–5). This observation is independent of the system’s absolute solidification velocity as the absolute velocities of CuZr are in the range of mm/s (Fig. 3), while those of NiTi, $(\text{Ni}_{0.3}\text{Cu}_{0.7})\text{Zr}$, $(\text{Ni}_{0.4}\text{Cu}_{0.6})\text{Zr}$, and $\text{Ni}(\text{Zr}_{0.5}\text{Ti}_{0.5})$ have values of cm/s (Figs. 4 and 5). For all $v(\Delta T)$ data points of a curve the frame rate of the HSC was kept constant, i.e., the scatter becomes larger with increasing velocity. Due to an accurate temperature measurement and a precise contactless triggering at a freely selectable undercooling, the scatter of the obtained velocity data is at least two orders of magnitude smaller than all measurements performed by former works.

In the case of CuZr (Fig. 3), ΔT_{hyp} is reached at an undercooling of $\Delta T = 230$ K. For $\Delta T < 230$ K the $v(\Delta T)$ data increase. For $\Delta T > 230$ K the slope of the $v(\Delta T)$ curve becomes negative and the velocity continues to decrease for higher undercoolings. The abrupt change in the $v(\Delta T)$ relation cannot be explained solely by $D(T)$ being dominant at high ΔT . For the eutectics $\text{Cu}_{0.56}\text{Zr}_{0.44}$ ($\Delta T_{\text{hyp}} = 339$ K, $\Delta T_{\text{max}} = 230$ K) and $\text{Cu}_{0.46}\text{Zr}_{0.54}$ ($\Delta T_{\text{hyp}} = 318$ K, $\Delta T_{\text{max}} = 270$ K), the hypercooling limit was not reached within the obtained undercooling range. Coming from intermetallic CuZr, one can see that shifting the composition by ± 4 at. % Zr engenders a drastic change of ΔT_{hyp} . Note that for both adjacent eutectic systems a similar behavior is observed for $\Delta T < \Delta T_{\text{hyp}}$.

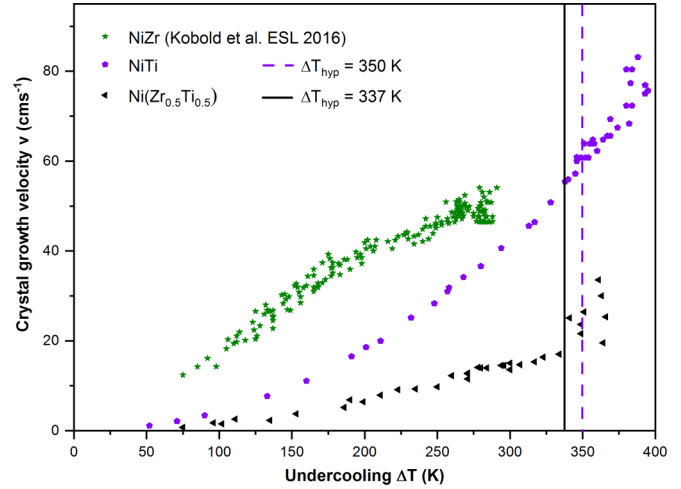


FIG. 5. Crystal growth velocity v as a function of the undercooling ΔT measured for intermetallic NiTi and the ternary alloy $\text{Ni}(\text{Zr}_{0.5}\text{Ti}_{0.5})$. NiTi exceeds the hypercooling limit significantly and shows a change in the $v(\Delta T)$ relation at ΔT_{hyp} . Therefore, the Ni-based ternary alloy was predestined for exhibiting similar effects as observed for the alloys $(\text{Ni}_{0.3}\text{Cu}_{0.7})\text{Zr}$ and $(\text{Ni}_{0.4}\text{Cu}_{0.6})\text{Zr}$. Both systems show a similar behavior for $\Delta T < \Delta T_{\text{hyp}}$ as the NiZr system, whose ΔT_{hyp} is not accessible [23].

Figure 4 shows the measured $v(\Delta T)$ data for the ternary alloys $(\text{Ni}_{0.3}\text{Cu}_{0.7})\text{Zr}$ and $(\text{Ni}_{0.4}\text{Cu}_{0.6})\text{Zr}$ in comparison to the binary alloy CuZr. For $(\text{Ni}_{0.3}\text{Cu}_{0.7})\text{Zr}$ the measured hypercooling limit is $\Delta T_{\text{hyp}} = 270$ K and for $(\text{Ni}_{0.4}\text{Cu}_{0.6})\text{Zr}$ it is $\Delta T_{\text{hyp}} = 280$ K. As for CuZr, a significant change in the $v(\Delta T)$ relation can be pinpointed to these hypercooling limits. For $(\text{Ni}_{0.3}\text{Cu}_{0.7})\text{Zr}$ we observe a power-law-like increase of $v(\Delta T)$ for $\Delta T < 270$ K and a constant $v(\Delta T)$ for $\Delta T > 270$ K. For $(\text{Ni}_{0.4}\text{Cu}_{0.7})\text{Zr}$ we also observe a power-law-like increase of $v(\Delta T)$ for $\Delta T < 280$ K and a significant fluctuation of the $v(\Delta T)$ data for $\Delta T > 280$ K. Note that for these systems we observe a fourfold solidification front in the HSC recordings for low undercoolings in the $\Delta T < \Delta T_{\text{hyp}}$ regime, which *continuously* evolves to a spherical shape with increasing undercooling in the intermediate regime of $\Delta T < \Delta T_{\text{hyp}}$ and is perfectly spherical at $\Delta T = \Delta T_{\text{hyp}}$. Its shape remains spherical in the high undercooling regime $\Delta T > \Delta T_{\text{hyp}}$. Thus, the abrupt changes of the $v(\Delta T)$ relations at ΔT_{hyp} cannot be explained by a *continuous* change of the morphology of the envelope of the growing crystal.

For $(\text{Ni}_{0.3}\text{Cu}_{0.7})\text{Zr}$ the solid part of the sample slightly enlarges during solidification from the undercooled liquid. This enlargement is measured optically in the HSC to 20 pixel at maximum. With a resolution of $30 \mu\text{m}/\text{pixel}$ this corresponds to an enlargement of ≈ 0.06 cm of the sample. For a sample with a diameter of 3.5 mm and the maximum growth velocity constant to $v = 3.5 \text{ cm s}^{-1}$ for undercoolings $\Delta T > \Delta T_{\text{hyp}}$ (Fig. 4), the recalescence time is $\Delta t \approx 0.1$ s. For the enlarged sample, this corresponds to a true velocity of $v = 4.1 \text{ cm s}^{-1}$. The error of $\Delta v = 0.6 \text{ cm s}^{-1}$ can be compared to the measurement accuracy of the velocity listed in Table I. For the other investigated alloys, no significant enlargements at the recalescences are observed.

Figure 5 shows the measured $v(\Delta T)$ data of intermetallic NiTi with a hypercooling limit of $\Delta T_{\text{hyp}} = 350$ K and the ternary alloy Ni(Zr_{0.5}Ti_{0.5}) with $\Delta T_{\text{hyp}} = 337$ K. Again, in both cases we can observe an influence on the $v(\Delta T)$ relation for $\Delta T > \Delta T_{\text{hyp}}$.

Within a nucleation study, Kobold *et al.* showed that for intermetallic NiZr $\Delta T_{\text{max}} = 300$ K is the highest undercooling achievable at a cooling rate of 34 K/s (vacuum of 10^{-7} mbar in the ESL) [23]. With $\Delta H_f = 14.73$ kJ/mol and $c_p = 42.6$ J/mol K one can calculate the hypercooling limit via Eq. (1) for congruently melting NiZr yielding an undercooling temperature of $\Delta T_{\text{hyp}} = 346$ K [24]. Therefore, ΔT_{hyp} was never reached for NiZr. Note that the kink in the velocity curve for NiZr at ≈ 175 K (Fig. 5) does not correspond to the hypercooling limit of the system. It has been attributed to a change of the solidification front geometry, which will be discussed in a subsequent publication.

Table I summarizes the values concerning the hypercooling limits of the investigated systems. Either values for ΔT_{hyp} were extracted from the TTPs ($\Delta T_{\text{hyp,exp}}$) and ΔH_f or c_p was calculated knowing one parameter or the hypercooling limits were theoretically determined ($\Delta T_{\text{hyp,calc}}$) from literature values for the enthalpies of fusion and the specific-heat capacities. ΔT_{max} names the maximum experimentally achieved undercoolings for the corresponding alloys. The measured values for $\Delta T_{\text{hyp,exp}}$ and ΔT_{max} are precise to ± 10 K according to the accuracy of the pyrometer. For every alloy, the velocity error at the maximum velocity was calculated based on the used HSC frame rate. Accordingly, these values represent the upper limit for the scatter of the velocity data of each alloy. For the purpose of clarity on the relative courses of the $v(\Delta T)$ curves, no error bars were added to the figures.

Although commonly observed in levitated liquid droplets, fluid flow needs not be taken into consideration for the experiments to influence the solidification velocity. In the ESL the electric field has no tangential component on the droplet and there is no current through the sample, no electric traction on the surface, and no electrohydrodynamic convection. Consequently, no convection is caused by the levitation force. Free convection due to density fluctuations can usually be neglected [25]. The dominating driving force for fluid flow in the ESL is Marangoni convection, which is caused by temperature gradients due to laser heating of the sample. Obviously, at the rotating samples investigated in this work, Marangoni convection is much less than at nonrotating spherical droplets because much weaker temperature gradients occur. Although maximum flow velocities of up to 5 cm s^{-1} were measured for droplets processed in the ESL [25], the time period between the laser turnoff and the onset of solidification is a multiple of the viscous damping timescale [25,26]. Thus, during free cooling of the sample the fluid flow quickly damps in the liquid cooling flank such that any residual flow velocities in these droplets would be very small at the time of the recalescence.

We want to state again that the change in the $v(\Delta T)$ relations in Figs. 3–5 can clearly be linked to the undercooling temperature at which 100% of the melt solidifies during recalescence, i.e., ΔT_{hyp} . In the following we present a pure phenomenological description of our observations on the macroscopic scale (Fig. 2): we define $T_{\text{cn}} = T_{\text{crystal}} - T_{\text{n}}$,

whereas T_{crystal} is the temperature of the growing crystal and T_{n} is the nucleation temperature. T_{cn} becomes larger with increasing ΔT because T_{crystal} remains constant for $\Delta T < \Delta T_{\text{hyp}}$ ($T_{\text{crystal}} = T_{\text{m}}$). For $\Delta T > \Delta T_{\text{hyp}}$, T_{crystal} does not reach T_{m} anymore during recalescence, i.e., $T_{\text{crystal}} < T_{\text{m}}$. To explain the observed abrupt changes in the $v(\Delta T)$ relations for NiTi (Fig. 5), CuZr (Fig. 3), and (Ni_{0.3}Cu_{0.7})Zr (Fig. 4) at ΔT_{hyp} , T_{cn} should change differently for the three cases, but regularly for $\Delta T > \Delta T_{\text{hyp}}$, compared to $\Delta T < \Delta T_{\text{hyp}}$. This should affect the driving force for solidification, which usually increases linearly for $\Delta T < \Delta T_{\text{hyp}}$. Consequently, exceeding ΔT_{hyp} should have an effect on $v(\Delta T)$. Thus, as the different cases [NiTi: increase, CuZr: decrease, (Ni_{0.3}Cu_{0.7})Zr: constant] for $\Delta T > \Delta T_{\text{hyp}}$ cannot be unequivocally connected to how T_{cn} changes, one has to consider also other (kinetic) factors for a microscopic explanation. However, for (Ni_{0.4}Ni_{0.6})Zr (Fig. 4) and Ni(Zr_{0.5}Ti_{0.5}) (Fig. 5), T_{cn} should be irregular due to the large scatter in $v(\Delta T)$ for $\Delta T > \Delta T_{\text{hyp}}$.

IV. OUTLOOK

We are convinced that the discovery of the effect of the hypercooling limit on the crystal growth velocity will influence the understanding of solidification processes under nonequilibrium conditions. Fields in which nonequilibrium processes play a dominant role will benefit from an improvement of existing growth models. In the field of climate research, precipitation models are essential in understanding the water cycle of the earth. Nonequilibrium solidification governs, for instance, the formation of hailstones or ice clouds [27].

In astrogeophysics, the structure and formation of meteorites provides insight into the genesis of our solar system. Remarkably, Nagashima *et al.* reproduced chondrules from levitated, hypercooled melts of forsterite (Mg₂SiO₄) in the laboratory [28]. Primitive meteorites are remnants of the solar nebula, containing intermixed rock and metal flakes. Chondrules are small spherical silicate inclusions in these meteorites, which were formed under ambient conditions of our early solar system. Thus, understanding the formation conditions of chondrules gives decisive information about the conditions which prevailed in the early period of our solar system.

V. SUMMARY AND CONCLUSION

We have investigated the crystal growth velocity as a function of the undercooling temperature for the glass-forming alloys NiTi and Cu–Zr, as well as for the Zr-based ternary alloys (Ni_xCu_{1-x})Zr ($x = 0.3, 0.4$) and the Ni-based ternary alloy Ni(Zr_{0.5}Ti_{0.5}) ($x = 0.5$) with an improved experimental setup, which allowed us to significantly reduce the scattering of the data and make small effects on the $v(\Delta T)$ curves visible. In contrast to previous publications on CuZr [5,6] we do *not* observe the $v(\Delta T)$ behavior as described in these publications. For all investigated systems we observe a crystal growth velocity which, for $\Delta T < \Delta T_{\text{hyp}}$, increases with a power law with increasing undercooling temperature and a decreasing (CuZr), a constant [(Ni_{0.3}Cu_{0.7})Zr] and scattering [(Ni_{0.4}Cu_{0.6})Zr, Ni(Zr_{0.5}Ti_{0.5})] behavior for $\Delta T > \Delta T_{\text{hyp}}$.

Since these behaviors show a clear connection to ΔT_{hyp} , we do *not* assume that the underlying effect is caused by glass-forming properties [CuZr, (Ni_{0.3}Cu_{0.7})Zr and (Ni_{0.4}Cu_{0.6})Zr]

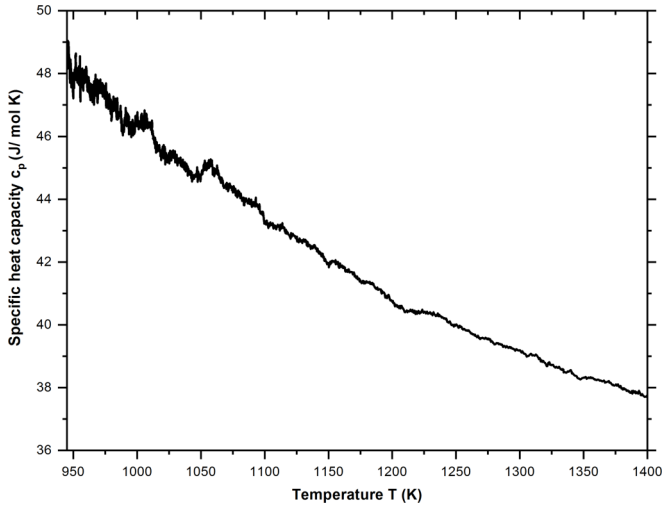


FIG. 6. Specific-heat capacity c_p as a function of temperature as calculated from the TTP of CuZr.

in the obtained undercooling regimes. The observed effect seems to be fundamental for alloy systems which exceed the hypercooling limit. To our understanding, this effect has not yet been addressed in any scientific work, even though several articles on hypercooling in combination with $v(\Delta T)$ analysis have been published [11,18,19]. With our results we could shed new light on the existing paradigm for the reason of the deceleration effect observed in the solidification velocity with increasing undercooling temperature in glass-forming systems. In general, this has far-reaching ramifications in various fields as diverse as materials science, climate research, and astrophysics.

ACKNOWLEDGMENT

The work at DLR was partly funded by ESA MAP MET-COMP Contract No. 14243/00/NL/SH.

APPENDIX A: EXPERIMENT

Figure 1 shows two frames from a HSC recording of the solidification process of CuZr. A small mirror, which is installed behind the levitating sample and in the line of sight of the HSC, makes it possible to pinpoint the onset and end of solidification to a single frame yielding a significant enhancement of the accuracy of the measured $v(\Delta T)$ data. In previous works, where $v(\Delta T)$ was determined with a HSC, only 50% of the sample surface were recorded. Note that in many cases the onset or end of solidification takes place at the part of the sample that is not visible. Therefore, the remaining 50% were linearly extrapolated [5,29]. However, for most intermetallic alloys the solidification front does not propagate with constant velocity over the sample surface, although the growth velocity of the crystal growing into the undercooled melt is assumed to be constant. This is due to the intersection between the spherical sample surface and the often complex geometry of the growing crystal [24]. Therefore, an extrapolation to the

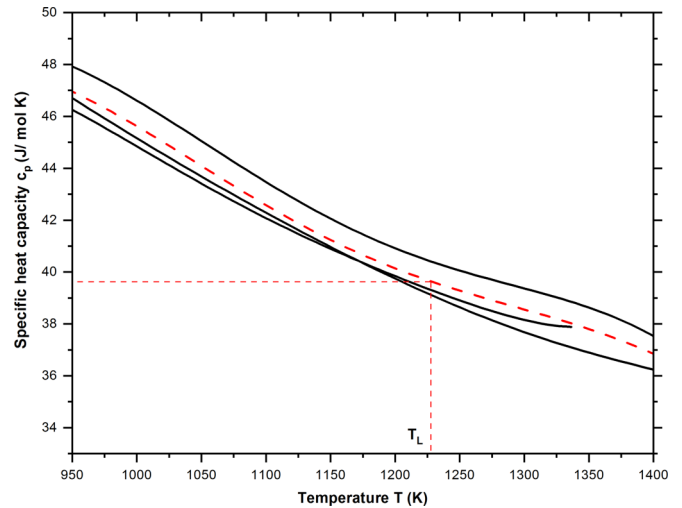


FIG. 7. Every black curve represents the average of three single c_p measurements for CuZr as seen in Fig. 6. The dashed red curve is an average of the three black curves in the diagram. The specific-heat capacity $c_p = 39.7$ J/mol K is marked at the liquidus temperature $T_L = 1226$ K of CuZr.

remaining 50% often leads to a large scatter, especially if the crystal geometry is unknown (as is the case for all investigated alloys in this work). The scatter can be significantly reduced in our setup, where we use a mirror in combination with a high frame rate.

APPENDIX B: RESULTS AND DISCUSSION

With Planck's law one can calculate the specific-heat capacity $c_p(T_L)$ at the liquidus temperature as described by Wessels *et al.* [30] via

$$c_p(T_L) = \frac{-\sigma_B A \epsilon_T (T^4 - T_0^4)}{m \frac{dT}{dt}} \quad (\text{B1})$$

with σ_B : Stefan-Boltzmann constant, A : sample surface area, ϵ_T : hemispherical total emissivity, T : temperature of the melt taken from the TTP, and T_0 : ambient temperature. Since the temperature dependency of ϵ_T is unknown, a material-specific constant value ($\epsilon_T = 0.28$) is used to calculate c_p . The cooling rate dT/dt is determined from the part of the TTP, where the sample cools down only by radiation of heat.

Table I summarizes the measured and calculated data relevant for the hypercooling limits of the systems. With literature values for ΔH_f and c_p at the liquidus temperature T_L derived via Eq. (B1) from data for the specific-heat capacity depending on the undercooling temperature the hypercooling limits were calculated. Exemplary, $c_p(\Delta T)$ curves are presented in Figs. 6 and 7 for the investigated CuZr. As notable, for CuZr the theoretically determined $\Delta T_{\text{hyp,calc}}$ and the experimentally determined $\Delta T_{\text{hyp,exp}}$ match perfectly. Furthermore, it becomes evident that the $\Delta T_{\text{hyp,calc}}$ values for the eutectic compositions $\text{Cu}_{0.56}\text{Zr}_{0.44}$ and $\text{Cu}_{0.46}\text{Zr}_{0.54}$ are higher than the maximum undercoolings ΔT_{max} reached in our experiments.

- [1] P. F. Paradis, T. Ishikawa, G. W. Lee, D. Holland-Moritz, J. Brillo, W. K. Rhim, and J. T. Okada, *Mater. Sci. Eng., R* **76**, 1 (2014).
- [2] J. Brillo, G. Lohöfer, F. Schmidt-Hohagen, S. Schmidt, and I. Egry, *Int. J. Mater. Prod. Technol.* **26**, 247 (2006).
- [3] D. M. Herlach, *Metals* **4**, 196 (2014).
- [4] D. M. Herlach, R. Kobold, and S. Klein, *JOM* **70**, 726 (2018).
- [5] Q. Wang, L.-M. Wang, M. Z. Ma, S. Binder, T. Volkmann, D. M. Herlach, J. S. Wang, Q. G. Xue, Y. J. Tian, and R. P. Liu, *Phys. Rev. B* **83**, 014202 (2011).
- [6] H. Wang, D. M. Herlach, and R. Liu, *Europhys. Lett.* **105**, 36001 (2014).
- [7] R. Kobold, W. W. Kuang, H. Wang, W. Hornfeck, M. Kolbe, and D. M. Herlach, *Philos. Mag. Lett.* **97**, 249 (2017).
- [8] Ch. Tang and P. Harrowell, *Nat. Mater.* **12**, 507 (2013).
- [9] M. D. Ediger, P. Harrowell, and L. Yu, *J. Chem. Phys.* **128**, 034709 (2008).
- [10] H. W. Wilson, *London, Edinburgh Dublin Philos. Mag. J. Sci.* **50**, 238 (1900).
- [11] M. E. Glicksman and R. J. Schaefer, *J. Cryst. Growth* **1**, 297 (1967).
- [12] M. E. Glicksman, in *Principles of Solidification* (Springer, New York, 2011), p. 432.
- [13] A. Schillings, Erstarrungsvorgänge reiner und binär legierter organischer Modellsubstanzen unter- und oberhalb der Hypercooling-Grenze, Dissertation, Rheinisch-Westfälische Technische Hochschule Aachen, 1999.
- [14] A. Manka, H. Pathak, S. Tanimura, J. Wölk, R. Strey, and B. E. Wyslouzil, *Phys. Chem. Chem. Phys.* **14**, 4505 (2012).
- [15] Y. Xu, N. G. Petrik, R. Scott Smith, B. D. Kay, and G. A. Kimmel, *Proc. Natl. Acad. Sci. USA* **113**, 14925 (2016).
- [16] T. Buttersack and S. Bauerecker, *J. Phys. Chem. B* **120**, 504 (2016).
- [17] T. Buttersack, V. C. Weiss, and S. Bauerecker, *J. Phys. Chem. Lett.* **9**, 471 (2018).
- [18] G. Wilde, G. P. Görler, and R. Willnecker, *Appl. Phys. Lett.* **69**, 2995 (1996).
- [19] T. Volkmann, G. Wilde, R. Willnecker, and D. M. Herlach, *J. Appl. Phys.* **83**, 3028 (1998).
- [20] G. Wilde, Makroskopische Eigenschaftsänderungen unterkühlter metallischer Schmelzen, Ph.D. dissertation, Technische Universität Berlin, 1997.
- [21] T. Meister, Aufbau und Regelung eines elektrostatischen Levitators, Dissertation, Ruhr-Universität Bochum, 2000.
- [22] T. Kordel, D. Holland-Moritz, F. Yang, J. Peters, T. Unruh, T. Hansen, and A. Meyer, *Phys. Rev. B* **83**, 104205 (2011).
- [23] R. Kobold, M. Kolbe, W. Hornfeck, and D. M. Herlach, *J. Chem. Phys.* **148**, 114502 (2018).
- [24] R. Kobold, Crystal growth in undercooled melts of glass forming Zr-based alloys, Dissertation, Ruhr-Universität Bochum, 2016.
- [25] R. W. Hyers, *Math. Syst. Theor.* **16**, 394 (2005).
- [26] S. Binder, P. K. Galenko, and D. M. Herlach, *J. Appl. Phys.* **115**, 053511 (2014).
- [27] H. R. Pruppacher, in *Microphysics of Clouds and Precipitation*, 2nd ed. (Springer, Dordrecht, 1997), pp. 659ff., 679ff.
- [28] K. Nagashima, K. Tsukamoto, H. Satoh, H. Kobatake, and P. Dold, *J. Cryst. Growth* **293**, 193 (2006).
- [29] H. Assadi, S. Reutzel, and D. M. Herlach, *Acta Math.* **54**, 2793 (2006).
- [30] V. Wessels, A. K. Gangopadhyay, K. K. Sahu, R. W. Hyers, S. M. Canepari, J. R. Rogers, M. J. Kramer, A. I. Goldman, D. Robinson, J. W. Lee, J. R. Morris, and K. F. Kelton, *Phys. Rev. B* **83**, 094116 (2011).
- [31] M. Krause, Messung thermophysikalischer Parameter unterkühlter Kupfer-Zirkonium-Schmelzen, Dissertation, Universität Bremen, 2002.